DEVELOPMENT OF A SUPERSONIC GAS JET BEAM PROFILE MONITOR

H. Zhang[1,#], V. Tzoganis[1,2], A. Jeff[1,3], C.P. Welsch[1]
[1]Cockcroft Institute and The University of Liverpool, Warrington, WA44AD, UK
[2]RIKEN, Nishina center, Wako-chi, Japan
[3]CERN, Geneva, Switzerland

Abstract

A supersonic gas jet beam profile monitor has been developed by the QUASAR Group at the Cockcroft Institute, UK. It creates a 45 degree supersonic gas curtain to interact with the primary beam, and then collect the generated ions to measure the transverse profiles of the primary beam. The gas curtain functions as a non-interceptive screen, which allows us to insert it into high energy, high luminosity and high power beams without worrying about the damage that normal screen would suffer.

Recently, a new movable gauge module has been implemented in the test stand. The purpose is to investigate the gas curtain density distribution in order to understand the jet better. In this contribution, we will briefly discuss the monitor and focus on the gas curtain measurement with the newly installed movable gauge module.

INTRODUCTION

For almost every particle accelerator used contemporarily, beam profile monitors are an essential tool to diagnose the characteristics of the particle beam such as beam centroids, sizes and emittance. Many methods have been widely used for many years, for example scintillating screens, wire scanners, optical transition radiation, synchrotron radiation and laser wire. Each method has its own benefits and specific parameter space over which it can be applied. Nowadays, for the next generation of high energy, high brightness and high power beams such as the High Luminosity Large Hadron Collider upgrade [1] and the European Spallation Source [2], new methods are required in order to survive the destructive nature of the beams. In addition, low-energy, low-intensity beams of exotic particles such as the proposed Facility for Antiproton and Ion Research (FAIR) [3] require new non-interceptive methods to minimize the influence of monitoring on the beam.

Previously, residual gas Ionization Profile Monitors (IPM) [4] and Beam Induced Fluorescence profile monitors (BIF) [5] have been used in these situations due to their non-invasive properties. However, for both methods, the measurement is usually in one dimension, which means two monitors are required for horizontal and vertical profile measurement. Since both methods rely on the residual gas density or pressure, accelerators operating in ultra-high vacuum will require a stable beam for long periods of time to accumulate sufficient signal. Normally, the BIF method requires much more time for integration under the same vacuum condition than the IPM method, but the latter can have poorer spatial resolution due to the ionization and collecting process; about 1.0 mm rms for positive ions and 4.0 mm rms for electrons has been reported by J. Krider [4] in one of the setup in Fermi National Accelerator Laboratory. A hydrogen jet [6] was also used to create a pressure bump in Brookhaven National Laboratory to diagnose their proton beam but the measurement was still limited to one dimension due to the large thickness of the jet.

Based on these gas-based methods, at the Cockcroft Institute we have developed a beam profile monitor using a thin supersonic gas jet [7,8]. In this paper, we will give a brief overview of the experimental setup and measurement principle. Together with the newly installed moveable gauge module, we will discuss the supersonic gas jet properties and the related resolution for this monitor.

EXPERIMENTAL SETUP

The whole setup of this monitor is shown in Fig. 1. In order to produce a supersonic gas jet, a 30 μm diameter nozzle was used in the nozzle chamber. Using a differential pumping technique, gas can flow through the nozzle from the gas cylinder with a high stagnation pressure (1-10 bars) to the low pressure area, the nozzle chamber (about 10^{-3} to 10^{-4} mbar in the pulsed operation). With such a large pressure decline, the gas enters the nozzle chamber without the sense of boundary condition and expands freely until a Mach disk is formed [9]. In this process, gas flow reaches a supersonic speed inside the Mach disk and then returns to a subsonic speed very quickly after the Mach disk. A conical skimmer (180 µm in diameter) is placed a short distance after the nozzle to accept the supersonic flow and collimate the flow. From the formula in [10], the distance between the nozzle exit and the Mach disk is proportional to the square root of the ratio of this stagnation pressure and nozzle chamber pressure. For our case it can be in the range of several tens mm. A 3D translation stage is attached to the nozzle to align the nozzle with skimmer as well as modifying the nozzle-skimmer distance to make sure the gas flow expands to supersonic speed and the Mach disk is not

#hao.zhang@cockcroft.ac.uk

ISBN 978-3-95450-176-2

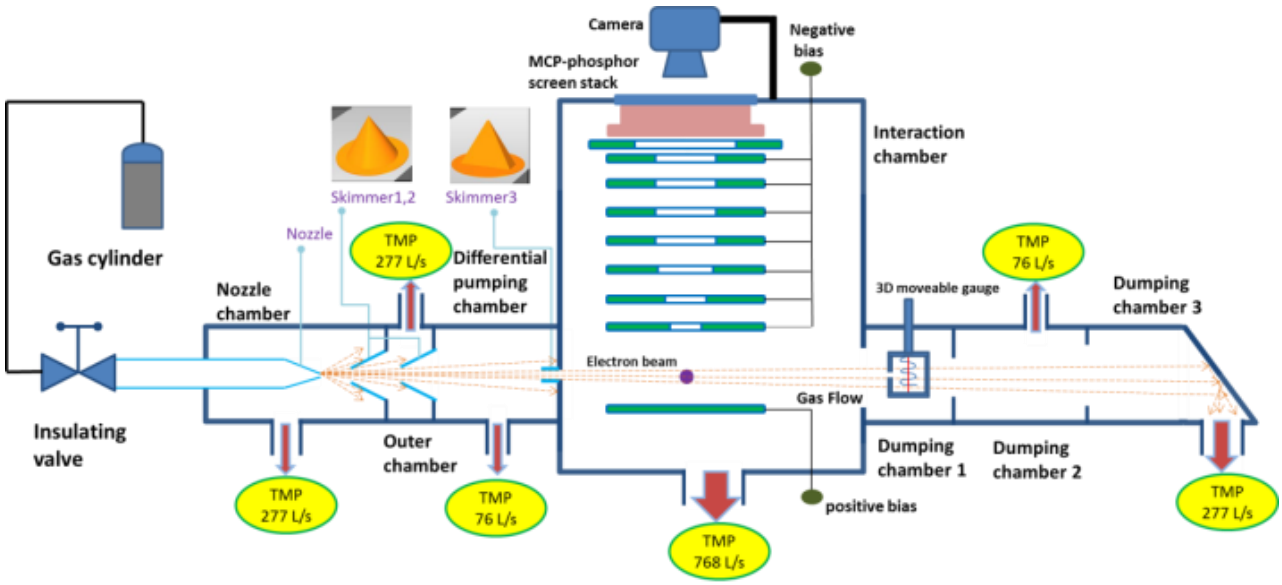

Figure 1: Schematic of the experimental setup

reached when the flow is collimated by the first skimmer. The gas loading is controlled by a pulsed valve with a sharp opening time on the millisecond level [10]. The formed supersonic gas jet is further collimated by a second conical skimmer (400 μm in diameter) which is positioned 25 mm from the first skimmer before the differential pumping chamber. The final collimation is done by a rectangular skimmer rotated by 45 degree with respect to the measured beam and placed at 325 mm from the first skimmer and before the interaction chamber. The jet is collimated as 45 degree screen in order to allow two-dimensional measurement. Two sizes of this third skimmer have been tested, 7.2×1.8 mm^2 and 4.0x0.4 mm^2. In normal operation the jet flows mostly across the interaction chamber and into the dumping chambers where it is pumped out by two turbo molecular pumps. In that way, the vacuum condition in the interaction chamber can be minimally affected.

Inside the interaction chamber a 3.5 keV electron beam was created and propagate perpendicular to the flow of the supersonic gas jet curtain. When collisions occur between the electron beam and the gas jet, the gas molecules will be ionized and then the produced ions will be accelerated by an external static electrical field. The field is generated by a series of hollow metallic electrodes biased at different potential levels to create a 12 kV/m potential gradient. After that, a Micro-channel plates and phosphor screen stack is implemented to amplify the ion signal and convert the signal to scintillating light which can be viewed by a CCD camera.

EXPERIMENTAL RESULTS FROM DIFFERENT THICKNESS JET CURTAIN

Previously, a larger third skimmer (7.2×1.8 mm^2) was used for preliminary tests as shown in Fig. 2. Since the size is relatively large, it makes the alignment relatively simple. In Fig. 3, we see images from both the gas jet and residual gas. The image from the gas jet is much brighter than that from the residual gas due to its higher localized density which increases the possibility for collisions to occur.

The Gaussian fit from the point of the maximum intensity gives a spot size of $\sigma_x = 0.42 \pm 0.02$ mm, $\sigma_y = 1.23 \pm 0.03$ mm for the gas jet image and $\sigma_x = 1.01 \pm 0.07$ mm for the residual gas image. The error here or for later Gaussian fit only shows the statistical error of the Gaussian fit with a 95% confidence bound, without considering the real resolution. The smaller size measured from the gas jet ions in the x direction is due to the smaller thermal spread of gas jet molecules compared with the residual gas, which is due to the low temperature characteristics of the supersonic gas jet. Normally the temperature of the supersonic gas jet is as low as few tens of degrees Kelvin. Along the y-axis, since residual gas fills the whole chamber, the image from the residual gas is limited only by the boundary of the metallic plates used to generate the extraction field. The increased brightness close to the edge illustrates the nonlinearity of the electric field close to the plates, which could degrade the resolution the monitor if the collision between the jet and electron beam happens near the fringe of the electric field. Another factor which affects the resolution particularly in the y axis is the thickness of the jet. For the jet curtain, since the larger skimmer is used, the thickness of the jet is at least 1.8/sin(45°) = 2.5 mm, which is much larger than the electron beam. In practice there is also an expansion of the jet after the final skimmer until the interaction point, so the thickness will be even larger. If we assume the measured beam size in y-axis will be the true size plus the jet thickness and regard the beam is equal sized in x and y axis, we can estimate roughly the jet thickness from the measurement. This assumption could be confirmed by an insertable phosphor screen directly measuring the electron beam which gives an approximately round beam shape. If we also assume the jet distribution is Gaussian.

ISBN 978-3-95450-176-2

We can calculate the jet thickness (RMS size) as $\sigma_y - \sigma_x$, we get a value about 0.81 mm. Notice the RMS jet thickness at the third skimmer is $2.5/2\sqrt{3}$ = 0.72 mm (uniform distribution assume here, which is most likely happen after the collimation). There is a 12.5% growth of the thickness.

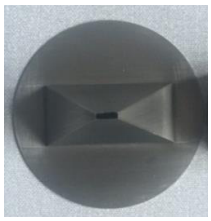

Figure 2: Picture of the previously used third skimmer with sizes 7.2×1.8 mm^2.

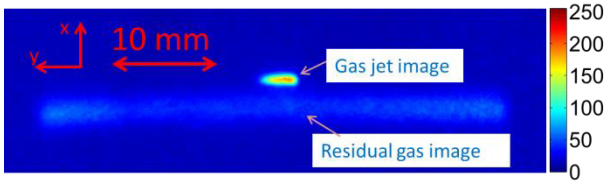

Figure 3: Images of the electron beam from both gas jet (larger size third skimmer) and residual gas.

Recently, a smaller rectangular skimmer (4×0.4 mm^2) has been installed to replace the larger size third skimmer as shown in Fig. 4. Although the alignment for this skimmer is more difficult, the curtain thickness can be considerably reduced. This will give a better resolution in the y axis which should allow a true 2-dimensional beam profile to be measured. As seen from the figure, the rotation angle is 32 degree due to limitations of the current mounting system. Fig. 5 is an example of this measurement with the same electron beam source. Note that some camera settings such as shutter time and gain have been changed to get a better image and the focus in the electron gun was also slightly changed thus measurements cannot be directly compared to each other. The Gaussian fit from the point of the maximum intensity gives a beam size σ_x = 0.56 ± 0.02 mm, σ_y = 0.53 ± 0.03 mm for the gas jet image and σ_x = 1.52 ± 0.07 mm for the residual gas image. For this measurement, since the beam size is comparable to the jet thickness (0.4/sin(32˚) = 0.75 mm), the previous assumption used to calculate the jet thickness is no longer applicable. Thus a detailed scan of the jet itself needs to be done using another method.

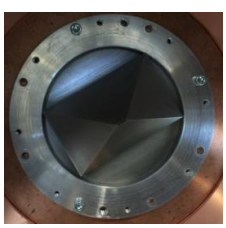

Figure 4: Picture of the newly third skimmer with sizes 4.0×0.4 mm^2.

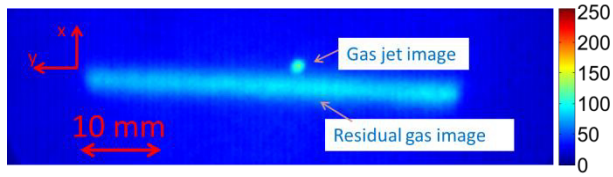

Figure 5: Images of the electron beam from both gas jet (smaller size third skimmer) and residual gas.

GAS JET DENSITY DISTRIBUTION MEASUREMENT

In order to understand the distribution of the gas jet curtain with the smaller skimmer, a moveable gauge module has been recently installed inside the first dumping chamber as shown in Fig. 1. The compression gauge concept [11] is used where the gauge is closed inside a small tube, with only a 2 mm slit open to accept the jet. The schematic of the compression gauge is shown in Fig. 6. Compared with a through gauge system, where there is no such closed tube, the surrounding pressure built up by the rest of the jet will not affect the measurement much. Here, we use a Granville-Phillips Series 274 Nude Bayard-Alpert Gauge. The whole module is attached to a 3D translation stage outside the vacuum chamber. The measured signal will be a time integration of the jet entering through the slit, and this signal will be amplified by a pico-ampere meter and then collected by a scope.

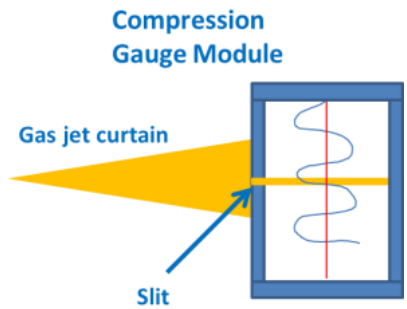

Figure 6: The schematic of the compression ion gauge module.

A typical measurement of the gas jet curtain from this gauge module is shown in Fig. 7. In the figure, the red curve indicates the trigger for pulse valve opening. The pulse width is 1.50 s. The blue curve represent the case when partial of the jet enters the compression gauge module through the slit, while the purple one shows the case that there is no jet entering the slit and the pressure bump is from the overall pressure change due to the jet flowing into the first dump chamber. Notice that in order to compare the two cases, the pressure curve shown here is the original pressure curve offset by the base pressure or the static pressure. It is clear that when there is a jet into the gauge module, the pressure rise follows the trigger immediately, because of the supersonic property of the jet; otherwise, the pressure rises more slowly.

ISBN 978-3-95450-176-2

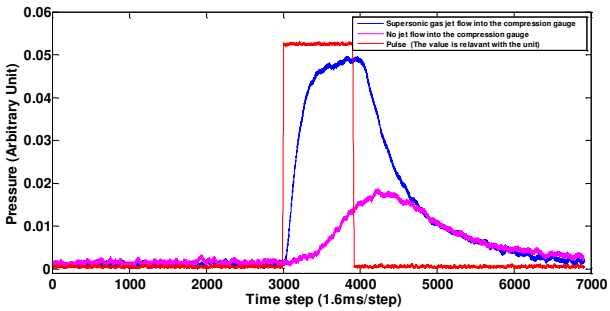

Figure 7: Measured pressure change of the moveable ion gauge.

Following the same procedure, we did a vertical scan across the gas jet. Pressure curves related to different vertical positions of the gauge are plotted in Fig. 8. For each curve, we acquire the maximum pressure and plot them in Fig. 9 against vertical position, thus giving a vertical distribution of the gas jet curtain. It can be seen that this distribution has a Gaussian shape, and a Gaussian fit shows that the gas curtain vertical distribution has RMS size of 1.01 ± 0.07 mm (one sigma), and the FWHM is 2.38 ± 0.17 mm. Considering that the vertical size of the skimmer is 4*sin(32°) = 2.12 mm, the collimated jet at this location will most likely be uniform and thus the RMS vertical size can be calculated as $2.12/2\sqrt{3}$ = 0.61 mm. Then the expansion of the curtain in vertical dimension over a long distance, i.e. from the 3rd skimmer to the moveable gauge which is about 560 mm, is rather small. This indicates that the jet is well collimated by the series of skimmers. By assuming the expansion is linear, we can obtain the vertical size of the jet.

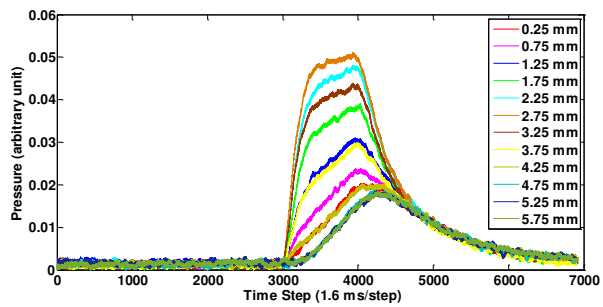

Figure 8: A vertical pressure scan of the gas jet from the moveable gauge module. Plots show the pressure curve at a few selected gauge positions.

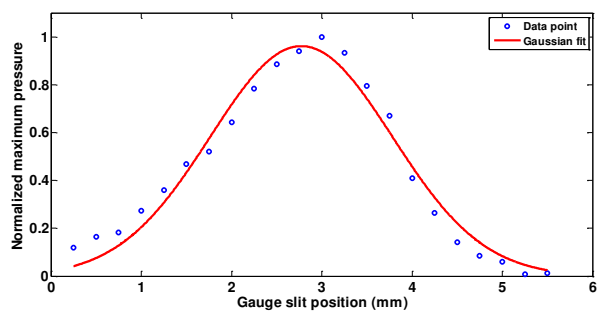

Figure 9: A vertical density distribution at the first dumping chamber.

To investigate the gas dynamics of the jet, we vary the distance between the nozzle and the first skimmer. Two measurements are made at each position: the jet pressure is measured with the moveable gauge module and the peak intensity from the gas jet image. The input pressure from the gas cylinder is kept at 5 bars and the pulse duration is kept at 1.5 seconds. For the jet pressure measurement we set the slit of the gauge module at the vertical position where the maximum density of the jet is achieved. Each data point represents the pressure rise for a specific nozzle skimmer distance as shown in Fig. 10. We can see that the pressure decays exponentially with a distance constant of about 3.76 mm. This decay is similar to the decay in gas density. Based on theory we assume that a pressure drop to one thousandth of the initial level indicates the position of the Mach disk, the latter is located at about 25.8 mm for the stagnation pressure.

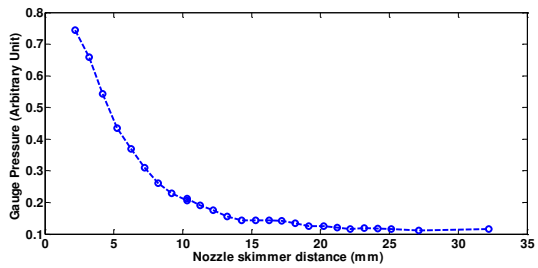

Figure 10: Plot of sampled supersonic jet pressure measured at the first dump chamber by the moveable gauge module versus nozzle to first skimmer distance.

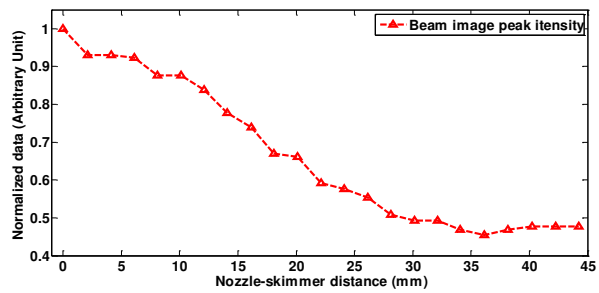

Figure 11: Plot of Peak intensity of the image from gas jet versus the nozzle to first skimmer distance.

From the peak intensity of the gas jet image with respect to the nozzle skimmer distance shown in Fig. 11, we see a quasi-linear decay of peak intensity and the Mach disk location should be larger than 30.0 mm. The formula describing the Mach disc [9]

$$X_M = 0.67 * d * \sqrt{\frac{P_0}{P_a}}$$

where X_M is the Mach disk location, d is the nozzle diameter (30 μm), P_0 is the stagnation pressure (5 bars), P_a is the boundary pressure inside the nozzle chamber (1.0e-3 mbar), then yields X_M = 45.0 mm. The measured Mach disk location is smaller than the theoretical value

ISBN 978-3-95450-176-2

because the theory does not include the skimmer itself which partially reflects the pressure wave and thus reduces the Mach disk distance.

CONCLUSION

In this paper we discussed recent progress on the supersonic gas-jet beam profile monitor. With a new third skimmer added the resolution in the y axis was greatly improved and allowed 2D measurement at the same time. A newly installed moveable ion gauge module opens the door for a detailed analysis of the factors affecting the resolution of this monitor, as well as a better understanding of the supersonic jet formation and dynamics.

Future developments will include a full 3D measurement of the jet, especially scans to study the thickness of the jet as a function of geometrical and thermodynamic parameters. These are key factors determining the achievable monitor resolution. Detailed comparison with the results from gas fluid simulations will then allow to benchmark simulation results and help to future improve the existing design for specific applications.

ACKNOWLEDGMENT

This work is supported by the Helmholtz Association under contract VH-NG-328, the European Union's Seventh Framework Programme for research, technological development and demonstration under grant agreement no 215080 and the STFC Cockcroft core grant No. ST/G008248/1.

REFERENCES

[1] R. Jones, E. Bravin, B. Dehning, T.Lefevre and H. Schmickler, 'Beam instrumentation and diagnostics for high luminosity LHC', *Proc. IPAC*, TUAC1, Richmond, VA, USA, 2015.

[2] A. Jansson, C. Böhme, B. Cheymol, H. Hassanzadegan, T. Shea and L. Tchelidze, 'Beam diagnostics for ESS', *Proc. IPAC*, New Orleans, Louisiana, USA, 2012.

[3] A. Peters and P. Forck, 'Beam diagnostics challenges in the FAIR project at GSI', *AIP Conf. Proc. 868*, 98 2006.

[4] J. Krider, 'Residual gas beam profile monitor', Nucl. Instrum. Methods Phys. Res., Sect. A, 278 (3),660-663, 1989.

[5] P.Forck, C. Andre, F. Becker R. Haseitl, and B. Walasek-Hohne, 'Beam induced fluorescence profile monitor developments', Proc. HB2012, WEO1C03 Morschach, Switzerland.

[6] T. Tsang, S. Bellavia, R. Connolly, D. Gassner, Y. Makdisi, M. Minty, T. Russo, P. Thieberger, D. Trbojevic, and A. Zelenski, "Optical beam profile monitor at the RHIC polarized hydrogen jet", *Proc. PAC09*, TH5RFP019, Vancouver, BC, Canada

[7] V. Tzoganis, C. P. Welsch, 'A non-invasive beam profile monitor for charged particle beams', Applied Physics Letters 104, 204104 (2014).

[8] V. Tzoganis, A. Jeff, C. P. Welsch, 'Gas dynamics considerations in a non-invasive profile monitor for charged particle beams', *VACUUM*, 109, pp. 417-424, 2014.

[9] H. Pauly, 'Atom, Molecule, and Cluster Beams I', Taylor & Francis, Berlin, 2000.

[10] H. Zhang, V. Tzoganis, A. Jeff, C. Welsch 'Development of a supersonic gas-jet monitor to measure beam profile non-destructively', *Proc. IPAC*, MOPWI006, Richmond, VA, USA, 2015.

[11] Y. Hashimoto, Y. Hori, T. Toyama, T. Fujisawa, T. Murakami, K. Noda, D. Ohsawa, 'Development of a Beam Profile Monitor using a Nitrogen-Molecular Jet for the J-PARC MR', *Proc. IBIC*, WEPF17, Oxford, UK, 2013.

ISBN 978-3-95450-176-2